Elaboration and characterization of molecularly imprinted polymer films based on acrylate for recognition of 2,4-D herbicide analogue

Ouahiba Beladghame, Nouria Bouchikhi, Djahida Lerari, Imad Eddine Charif, Olivier Soppera, Ulrich Maschke, Lamia Bedjaoui-Alachaher

Elaboration and characterization of molecularly imprinted polymers films based on acrylate for recognition of 2,4-D herbicid analogue

Ouahiba Beladghame [1], Nouria Bouchikhi [1,2], Djahida Lerari [2,3], Imad Eddine Charif [4], Olivier Soppera [5], Ulrich Maschke [6]&Lamia Bedjaoui-Alachaher [1*].

[1] *Laboratoire (LRM), Université de Tlemcen (UABT), BP119, 13000 Tlemcen, Algérie.*

[2] *Centre de Recherche (CRAPC). BP 384, zone industrielle 42004 Tipaza, Algérie*

[3] *Laboratoire (LSMTM), Université Houari Boumediene, BP 32, El-Alia, 16111 Bab-Ezzouar, Alger, Algérie.*

[4] *Laboratoire (LATA2M), Université de Tlemcen (UABT), PB 119, Tlemcen 13000, Algérie.*

[5] *Institut (IS2M)UMR 7361, F-68100 Mulhouse, France*

[6] *Unité (UMR CNRS N°8207), Bâtiment C6, Université de Lille - Sciences et Technologie, 59655 Villeneuve d'Ascq Cedex, France*

Corresponding Author:

Email: lamia.alachaher@univ-tlemcen.dz

Elaboration and characterization of molecularly imprinted polymers films based on acrylate for recognition of 2,4-D herbicid analogue

Abstract

This work reports the elaboration of novel molecularly imprinted polymers (MIPs) films by non-covalent approach in presence of phenoxypropionic acid (PPA) as 2, 4-D herbicid analogue. The MIPs were prepared by photo-polymerization of a mixture containing the n-butylacrylate (BuA) as monomer, 1, 6 hexanedioldiacrylate (HDDA) as crosslinking agent, template (PPA), 2-hydroxy-2- methyl-1-phenyl-propane-1-one as photoinitiator and chloroform as porogen solvent. The computer modelling and ^{1}H-NMR analysis confirmed the presence of non-covalent hydrogen-bonding interactions between the template molecule and the monomer in pre-polymerization complex. Imprinted and non-imprinted polymers (NIPs)were characterized by means of infra-red (IR) spectroscopy, thermogravimetric analysis (TGA) and atomic force microscopy (AFM) techniques. The template extraction of MIP and the recognition properties of the NIPs and MIPs were performed by gas chromatography (GC). The binding characteristics of MIPs and template were evaluated using equilibrium binding experiment and compared with the respective NIPs. For a maximum specific binding certain factors like amount of polymer film, concentration template and crosslinking density were altered. In every cases, the binding experiment showed that PPA imprinted polymer had better recognition ability than that of non-imprinted one. As result, MIP gave higher imprinting effect at higher crosslinking density and lower PPA concentration when using 6 mg of mass of polymer film.

Key words: Acrylate; Molecular imprinting; Dummy template; Thin film; Imprinting factor.

Introduction

Detection and adsorption of trace level of pesticides residues have attracted much attention in recent years, owing to their toxicity and health hazards. Indeed, due to the widespread use of various insecticides, fungicides, and herbicides in agricultural fields, residues of these chemical products have been found in soil, drinking water, and agricultural products[1, 2].One of the most widely used herbicides is 2,4-dichloro-phenoxyacetic acid (2,4-D), which acts as a growth plant regulator[3, 4].

However, due to its endocrine disrupting activities and cancer risk, its presence in food and the natural environment can cause serious harm to humans and animals [5-7]. As the World Health organization WHO has set the maximum contaminant limit for 2,4-D in drinking water at 30µg/L[8], sensitive methods for detecting residual 2,4-D are critical. HPLC and GC/MS methods have traditionally been used to monitor the presence of 2,4-D in the environment [9, 10].

These methods have some drawbacks, including high costs, sample pretreatment (derivatization), and time requirements. To overcome these main limitations, molecularly imprinted polymers (MIPs) were used to detect 2,4-D in a more efficient and sensitive manner.

The technology for obtaining MIPs is based on the formation of a complex between a template and a functional monomer in a selected solvent that acts as a porogen. The complex is then polymerized trough thermal or photo-initiation in the presence of a cross-linker and three-dimensional polymer network is formed. The template is removed from the polymer structure leading to the formation of specific binding sites [11]. The recognition of template molecule is based on the presence of cavities left, in MIPs materials after the removal of the template molecule. These cavities are complementary to the template molecules in terms of shape, size, and location of functional groups[12, 13].The use of MIPs for 2,4-D selective detection provides a slew of benefits, including very high specificity, very sensitive detection, and reusability of these polymers due to their remarkable stability.

Recently, special attention has been given to the use of MIPs in food quality control for efficient extraction of pesticide residues due to their specificity and sensitivity. In fact, many sensors have been successfully developed as pesticide detection materials mainly via electrochemical and optical responses, amongst others. in this contexte Fungicides and pesticides such as were well detected by Bitar et al. (2019) and Fang et al. (2017), using MIP hydrogels obtained be means of sol-gel or one-step polymerization methodologies.

These MIPs materials are generally made using methacrylic esters and vinylpyridine as functional monomers, which can be polymerized under thermal or UV light [14] in presence of dimethacrylate as crosslinking agent. The MIP formats may differ depending on the polymerization process: bulk polymerization produces after grinding monolithic materials, irregular particles whereas suspension polymerization [15], precipitation polymerization [16] and emulsion polymerization[17] produces well defined spherical particles.

The actual challenge is the conception of MIP in a thin film format to use them in miniaturized analysis system and sensors [18-20]. This can be done by spin coating [21] or sandwich method [22] among many others technics. The former method allows a production of thin films of controlled thicknesses but usually requires a

viscous pre-polymerization mixture. When more volatile solvent and monomers are used, the sandwich technique was preferred.

Good adsorptive capacities were frequently achieved by preparing MIPs in monolith or beads formats but the drawback is that the template extraction is incomplete, compared to the thin film format which shows more efficient target removal. Often if the imprinted molecule (template) is toxic and expensive, it can be substituted by cheaper and non-harmful analogous. Moreover the "dummy template" is used to avoid hindering the accurate and precise assay of the template when working at low concentration [23-25].

Attempts were made previously to imprint herbicides in polymers but the conventional synthesis needs a high concentration of crosslinking agent to produce rigid structure which does not allow the template molecule or "dummy template" to move freely [26-34]. So the extraction of imprinted molecule cannot be done totally and its diffusion within the polymer could be difficult.

In this present work, a new MIP thin film with low crosslinked polymer based, for a first time on acrylic monomer and crosslinker, was developed and characterized. The ability of these materials to recognize 2,4-D analogue was assessed using GC as an analytical method.

The paper deals with the elaboration of MIP films by radical photopolymerization of mixture containing the n-butylacrylate (BuA) as monomer, 1, 6 hexane diol diacrylate (HDDA) as a crosslinking agent and 2-hydroxy-2-methyl-1-phenyl-propane-1-one as a photo-initiator. The chosen dummy template is 2-phenoxy-propionic acid (PPA), which is analogous to the herbicide (2, 4-dichlorophenoxyacetic acid). The imprinted polymers were prepared by non-covalent method in the presence of chloroform as porogen solvent. Non imprinted polymers (NIPs) were also prepared by the same procedure without the template molecule. The prepolymerization complex between a template and monomer through hydrogen bonding interaction was investigated by computer modelling and confirmed by ^{1}NMR spectroscopy.

Non- imprinted polymers (NIPs) and imprinted polymers (MIPs) were characterized by infrared spectroscopy, thermogravimetric analysis (TGA) and atomic force microscopy (AFM). The recognition properties of the NIPs and MIPs materials obtained toward PPA were evaluated by GC technique using the batch binding method. Factors affecting the rebinding were also discussed. The obtained results showed a specificity of printed materials.

Experimental part

Reagents and chemicals

n-Butylacrylate (nBuA), 1,6-Hexanediol diacrylate (HDDA), chloroform (99%), Ethanol (99%) and Acetonitrile (ACN) (99%) were all provided by Sigma Aldrich. 2-Hydroxy-2 -methylpropiophenone (Darocur) 1173 (97%) and 2-phenoxypropionic acid (PPA) (98%) were purchased from Ciba. The chemical structures of main reagents are illustrated in Fig. 1. All reagents were used without further purification.

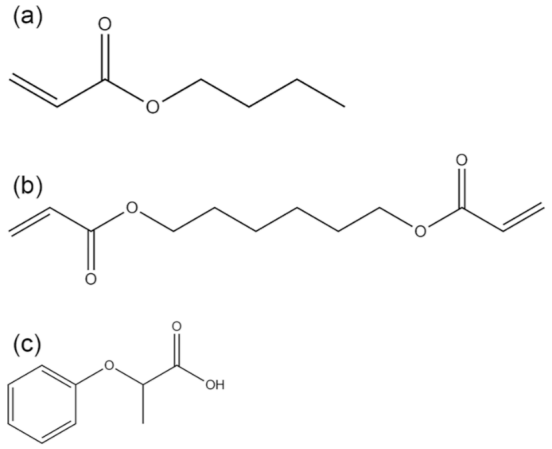

Fig. 1 Chemical structures of reagents, **a** n-butyl acrylate, **b** 1,6-hexanediol diacrylate, and **c** 2-phenoxypropionic acid

Methods and instruments

Modelling and simulation

All calculations were performed with the Gaussian 09 package [35]. The most stable geometries of all species (monomer, template, complex) were obtained using density functional theory DFT-B3LYP/6-31G (d,p) [36].

The binding energy for analysis of the hydrogen bonding interaction is obtained using the following equation:

$$\Delta E = E(\text{complex}) - [E(\text{template}) + E(\text{monomer})] \quad (1)$$

E (complex) is the total energy of the template-monomer; E (template) and E (monomer) are the total energies of the template and the monomer respectively.

The stabilization interaction energy $E_{i\to j^*}^{(2)}$ were performed using natural bond orbital (NBO 3.1) program implemented in the Gaussian 09 package at the DFT/B3LYP/6-31G(d,p) method [37]. The second-order perturbation interaction energy $E_{i\to j^*}^{(2)}$ represents the estimate of non-covalent bonding-anti-bonding interaction.

$$E_{i\to j^*}^{(2)} = -n_i \frac{\langle \sigma_i / \hat{F} / \sigma_j^* \rangle^2}{\varepsilon_{j^*} - \varepsilon_i} \quad (2)$$

Where, n_i is the donor orbital occupancy, ε_i and ε_{j*} are orbital bonding and anti-bonding energies and $\hat{F}$ is the off-diagonal NBO Fock matrix element. σ_i and σ_j^* are the respective donor and acceptor natural bond orbitals.

Infrared spectroscopy

Fourrier transform infra-red (FTIR) spectra were obtained by means of an Attenuated Total Reflectance (ATR) technique using Agilent Cary 640 instrument spectrometer. All measurements were taken at room temperature. FTIR spectra were recorded over the range 500 – 4000 cm^{-1} at 2 cm^{-1} resolutions and represented an average of 32 scans.

^{1}H-NMR analysis

^{1}H-NMR analysis were conducted on a BrukerAvance III 400 NMR US + spectrometer (300Hz) with 16 scans, at 300K, using the deuterated chloroform ($CDCl_3$) as solvent and tetramethylsilane (TMS) as an internal reference. The ^{1}H-NMR spectra were analyzed with Masternova software.

Thermogravimetric analysis

Thermogravimetric analysis (TGA) was performed using TGA LINSES PT1600 STAATG/DSC.The analysis of the sample with an average mass of 5mg was carried out under air atmosphere from 25 to 700°C, at a heating rate of 10°C/min.

Atomic force microscopy (AFM) analysis

Atomic force microscopy (AFM) analysis of the thin films was conducted using a Flex- AFM (nanosurf), operated on the tapping mode. The scanning head is connected to the C3000 controller working at resonance frequency < 4 MHz. The Flex AFM video option integrates two cameras for a parallel top and side view, which allows to quickly find an area of interest and bring the cantilever closer to the surface before the final approach. The areas of 2x2 µm² size was scanned for all samples and the obtained images were treated by using the image processing Gwyddion software.

Films elaboration

NIPs and MIPs were prepared in the absence and in the presence of the template respectively. Several formulations were prepared to show the impact of crosslinking agent quantity in the presence and absence of solvent, on the physico-chemical properties and the recognition efficiency of resulting polymers.

The compositions of mixtures are described in Table 1. Imprinted and non-imprinted films were produced using the sandwich method. For this purpose, a glass mold of 10 x 10 mm² and a thickness of 0.13 mm was fabricated. Next, 80 µL of pre-polymerization solution was deposited onto the center of glass slide which was covered immediately by polyethylene terephthalate (PET) film (with a thickness of 23 µm) to avoid the inhibiting effect of oxygen. Finally, the whole was put under UV radiation (λ = 365 nm, I_0 = 0.7 mw/cm^2) for 10 min and 15 min for the NIP and MIP films, respectively. The resulting films have a thickness of around 80 µm.

Table 1 Composition of MIPs and NIPs formulations

Series	Polymer films	Mixture PPA:BuA:HDDA (mol%)	Mixture:$CHCl_3$ (Volume ratio)
1:NIPs	NIP1a	0:4:4	3:1
	NIP2a	0:4:8	
	NIP2b	0:4:8	
2:MIPs	MIP1a	1:4:4	3:1
	MIP2a	1:4:8	
	MIP2b	1:4:8	

Detection of PPA using gas chromatography– flame ionization detector (GC–FID)

Removal of PPA from MIP films was performed using the gas chromatography GC (Clarity softwares) coupled to a flame ionization detector FID.

The GC chromatogram of PPA solution containing an internal standard was obtained using a Teknokroma TRB-5 column (a length of 30 m, a 0.32 mm inner diameter, a 0.1 µm film thickness). The temperature program of the GC oven was as follows: initial temperature of 60°C held for 3 min, a heating rate of 13°C/min to 190°C followed by a hold of 3 min. The temperature of the injector used in split mode was adjusted to 250°C. The flow rate of nitrogen, used as the carrier gas, was 1mL/min and the time analysis was about 15 min.

Calibration curve for PPA was constructed by chromatography of six acetonitrile solutions containing different concentrations (0.2–2.0 mg/mL) of PPA and a constant concentration (0.25 mg/mL) of the internal standard heptanol; 0.5 µL of each solution was injected into the GC system.

GC calibration plot was obtained by least-squares linear regression analysis of the peak-area ratio y of PPA/heptanol against concentration, x, of PPA. The plot was linear in the studied range; its corresponding equation was y = 0,7995x - 0,0391 with correlation coefficient R^2 = 0,9956.

For PPA extraction, the resulting MIPs films were immersed in a washing solution of acetonitrile-ethanol (90/10) (v/v) for 2 hours at room temperature. After drying the supernatant, 6 µL of heptanol dissolved in 1 mL of acetonitrile were added and the whole was analysed by GC. The procedure was repeated several times changing the washing solution every two hours. The washed MIP (wMIP) were obtained when no PPA was detected by GC.

The choice of the washing solution is based on the ability of the solvent to diffuse within the polymer and to take off the target. As acetonitrile is an aprotic solvent, it does not allow the complete extraction of the PPA and it remains "stuck" in the network. The modification of the composition of the washing solutions was achieved by adding 10% by volume of ethanol to the ACN solution to promote the removal of the PPA [38].

The dashed line in Fig. 2 corresponds to the first wash of MIP2a. It shows a chromatogram of PPA solution in presence of heptanol as internal standard and acetonitrile as a solvent where any interference has been noted.

The release of PPA from the MIPs was obtained by monitoring the disappearance of characteristic peak at 12, 64 min. So the solid line in Fig. 2 exhibits the complete PPA disappearance, after the last wash indicating that the template was completely removed from MIP2a films.

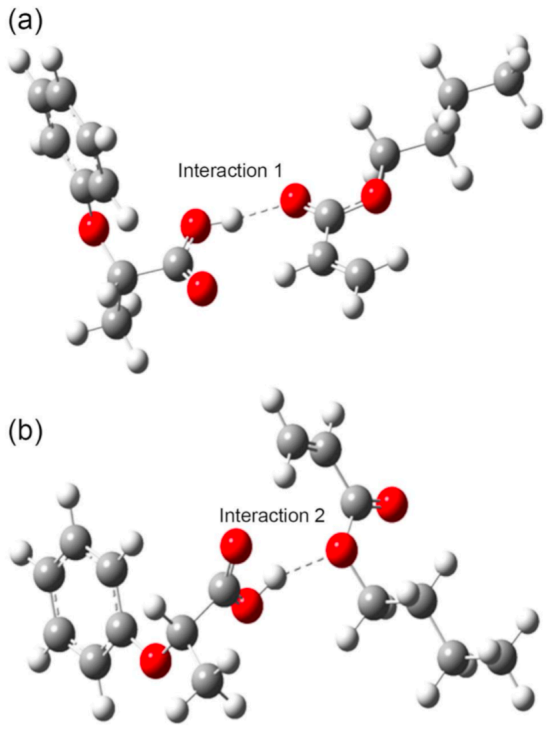

Fig. 2 DFT-B3LYP/6-31G (d, p) optimized geometries of the complexes 1 (**a**) and 2 (**b**). (Oxygen atoms in red, carbon atoms in gray, hydrogen atoms in white)

Results and discussion

Monomer-target interaction

The key step in the molecular printing process is the formation of a pre-polymerization complex between the template molecule and the functional monomer. Molecular modeling, infrared, and ^{1}H-NMR analysis were used in this study to assess the formation of intermolecular hydrogen bond in the complex between the template molecule PPA and the functional monomer BuA.

Natural bond analysis

In the molecular printing, molecular modeling is widely used to predict the formation of the pre-polymerization complex (template-monomer) between monomers and the template molecule. The Fig.3 shows two possibilities of interaction. Complex 1 presents the carbonyl C=O of monomer and acidic proton of PPA interaction while complex 2 corresponds to C-O of monomer and acidic proton of PPA interaction.

According to Table 2, after combining with the functional monomer, the bond length of the template's hydroxyl group (OH) increases from 0.975 to 0.995 Å in complex 1 and to 0.987Å in complex 2. On the other hand the complex 1 has a shorter hydrogen bond length $r_{O...H}$ (1.758 Å) than of complex 2 (1.873 Å). Consequently, the hydrogen bonding interaction formed in complex 1 between the acidic proton and the oxygen atom of the functional monomer carbonyl group is stronger than that formed in complex 2 with the oxygen atom of the ester group.

Table 2 Computational modeling data for complexes template-monomer 1 and 2: binding energy, ΔE (kcal/mol), and bond length, *r* (Å)

	r_{O-H}	$r_{O...H}$	Binding energy (ΔE)	Stabilization energy ($\Delta E^{(2)}$)
Template	0.975			
Complex 1	0.995	1.758	−14.18	LP(2 s) $O_{(C=O)} \rightarrow \sigma^*_{OH}$: 9.16 LP(2p) $O_{(C=O)} \rightarrow \sigma^*_{OH}$: 16.16
Complex 2	0.987	1.873	−9.22	LP(2 s) $O_{(C-O)} \rightarrow \sigma^*_{OH}$: 10.74 LP(2p) $O_{(C-O)} \rightarrow \sigma^*_{OH}$: 2.98

The binding energies of complexes 1 and 2 are shown in Table 2. Since the lower binding energy leads to a more stable complex, the hydrogen-bond in complex 1 (-14.18 kcal/mol) plays more important role than in complex 2 (-9.22 kcal/mol).

To simplify notation, numbers are assigned to the hydrogen bonding interaction, as represented in Fig.3. According to the NBO, interaction 1 involves the valence electron lone pairs (LP (2s), LP (2p)) of oxygen atom of C=O group of monomer and anti-bond orbital of O-H bond (σ^*_{OH}) of PPA. Interaction 2 involves the electron lone pairs (LP (2s), LP (2p)) of ester group oxygen atom of monomer and anti-bond orbital of O-H bond (σ^*_{OH}) of PPA. The stabilization energies $E^{(2)}$ of these two interactions are given in Table 2. As can be seen, the

stabilization $E^{(2)}$ energy caused by $LP(2p)O_{(C=O)} \rightarrow \sigma^*_{OH}$ interaction 1(16.16 kcal/mol) is greater than that of $LP(2p)\ O_{(C\text{-}O)} \rightarrow \sigma^*_{OH}$ interaction 2 (2.98 kcal/mol). The orbital interactions involving the first lone pair LP (2s) of oxygen atom are similar in both complexes (~10 kcal/mol). According to this result, the interaction 1 (complex 1) is supposed to form a stable complex.

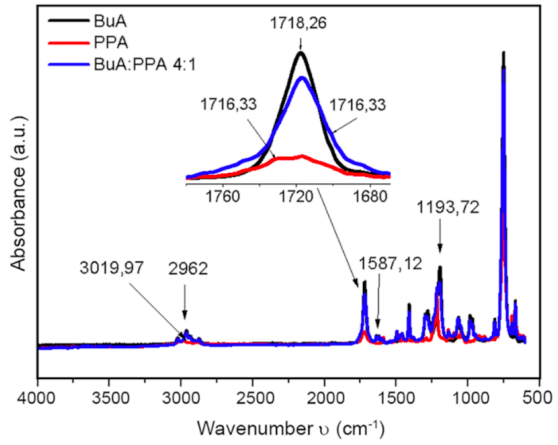

Fig. 3 IR spectra of BuA, PPA and mixture of BuA:PPA 4:1 in chloroform in the range of 500–4000 cm^{-1}. The insert shows the absorption band of C=O in the range of 1680–1780 cm^{-1}

Infrared spectroscopy analysis

Interaction studies were also carried out by ATR-FTIR and ^{1}H-NMR spectroscopies but in this case using a minimum volume of chloroform to better dissolve the monomer and PPA mixture. The choice of this solvent and of its added volume have been recommended in order to avoid destroying the interactions established previously, in the complex. Furthermore, chloroform has a low dielectric constant (4.8) which promotes the formation of hydrogen bond donor-acceptor complexes [42] Piletska, E. V., Guerreiro, A. R., Whitcombe, M. J., & Piletsky, S. A. (2009). Influence of the polymerization conditions on the performance of molecularly imprinted polymers. *Macromolecules*, *42*(14), 4921-4928 Karlsson, B. C., O'Mahony, J., Karlsson, J. G., Bengtsson, H., Eriksson, L. A., & Nicholls, I. A. (2009). Structure and dynamics of monomer− template complexation: an explanation for molecularly imprinted polymer recognition site heterogeneity. *Journal of the American Chemical Society*, *131*(37), 13297-13304..In this context, it was clearly evidenced that lowering the dielectric constant of the porogenic solvent utilized for the complexation between the monomer and template molecule increased the uptake efficiency. (Water, acetonitrile, chloroform, and toluene have respective dielectric constants of 80, 37, 4.8, and 2.3). The authors explain these results by the different polarity of the solvent which has an impact on the interactions between the model molecule and the functional monomer. These interactions have a significant impact on the structure of the imprinting sites in the MIP. Solvents with high polarity show maximum interactions with template and functional monmer, which reduces their chances of interacting to form suitable imprinting sites. Amaly, N., Istamboulie, G., El-Moghazy, A. Y., & Noguer, T. (2021). Reusable

molecularly imprinted polymeric nanospheres for diclofenac removal from water samples. *Journal of Chemical Research*, *45*(1-2), 102-110

From interaction studies by NBO, BuA monomer-PPA template (M/T) ratio of 1:1 was sufficient although some evidence did suggest that additional interactions may be also occurring at high M/T ratio. Based on these findings, ATR-FTIR and ^{1}H-NMR spectroscopies were used to investigate the interaction of BuA and PPA at 4:1 ratio which is the most commonly used for non-covalent interactions and has frequently resulted in improved MIP selectivity [39-41]. The shift of hydrogen donors and acceptors bands are used to identify the formation of hydrogen bonding in FTIR characterization [21, 43, 44].

Fig.4 shows the ATR-FTIR spectra of BuA monomer, PPA template and the BuA:PPA mixture with molar ratio 4:1in chloroform.

The ATR-FTIR spectra of BuA shows principally the C=O stretching vibrations band at1718,26 cm^{-1},the characteristic bands of C-O groups at1193,72cm^{-1} and the aliphatic stretching of the C-H bond appeared at 2962cm^{-1}.

In the PPA spectra, the C=O stretching vibrations band appears at 1716,33 cm^{-1},the absorption of the aromatic C=C bond is observed at 1587,12 cm^{-1} and the band at 3019,97 cm^{-1} represents the OH stretching vibrations.

In the case of BuA/PPA mixture, the intensity of C=O stretching vibration band of BuA decrease and shifts to 1716,33cm^{-1}.This slight decrease of wavenumber and intensity is most likely the result of intermolecular hydrogen bonding between the carboxylic groups of PPA and the carbonyl groups of BuA [12].

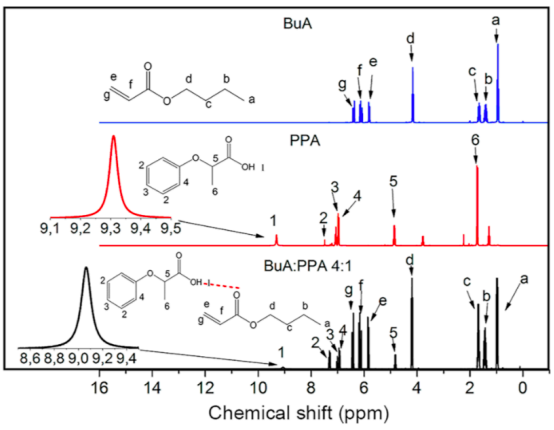

Fig. 4 ^{1}H NMR spectra of BuA, PPA, and mixture of BuA:PPA 4:1 in $CDCl_3$

^{1}H-NMR study

NMR characterization is widely used in non-covalent imprinting systems to study the monomer-template interaction. Because of local changes in the electronic environment, the interaction is characterized by a chemical shift in NMR spectra.

The ^{1}H- NMR spectra of BuA, PPA and a mixture of BuA:PPA with molar ratio (4:1) in $CDCl_3$ were presented in Fig. 5 and the chemical shifts of all protons were gathered in Table 3.

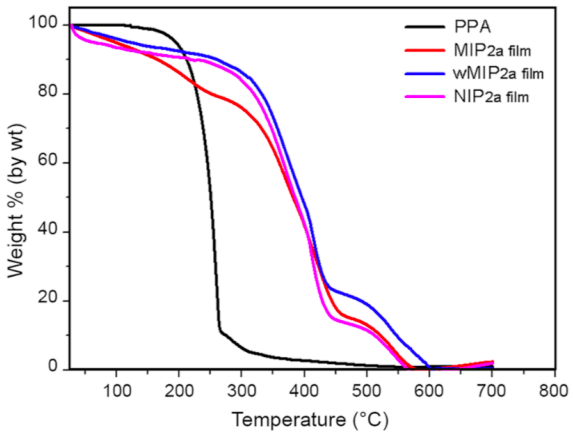

Fig. 5 Thermogravimetric analysis curves of MIP2a, NIP2a, wMIP2a and PPA

Table 3 Proton chemical shift (ppm) of BuA, PPA, and mixture of BuA:PPA 4:1 in $CDCl_3$

	Chemical shift (ppm)		
	PPA	BuA	BuA:PPA 4:1
H1 (s)	9.31		9.06
H2 (s)	7.49		7.33
H3 (t)	7.06		7.00
H4 (d)	6.98		6.94
H5 (m)	4.85		4.83
H6 (d)	1.73		
Ha (t)		0.94	1.00
Hb (m)		1.42	1.42
Hc (m)		1.68	1.67
Hd (t)		4.16	4.16
He (d)		5.79	5.85
Hf (m)		6.13	6.19
Hg (d)		6.36	6.40

s singlet, *d* doublet, *t* triplet, *m* multiplet

The signal at 9.31 ppm is assigned to the deshielded proton of the carboxylic acid group (Figure 5 and Table 3). The addition of BuA molecules resulted in a slight shielding effect, shifting the signal to 9.06 ppm. This is very likely due to the formation of hydrogen bonds between the BuA monomer ester group and the PPA carboxylic acid group. In other words, a successful complex formation is suggested, as supported by the work of Vendamme at al [45].

Polymers characterization

IR analysis of films

IR characterization was carried out to demonstrate the consumption of the monomer's characteristic C=C double bond during photo-polymerization and to determine the functional groups present in the MIP films before and after washing.

Fig. 6 depicts the IR spectra of a NIP2a mixture and the resulting NIP2a film as typical examples. In the NIP2a mixture and NIP2a film spectra, the band centered on 2946 cm^{-1} is relied to the deformation vibrations of ($–CH_3$) groups and the strong absorption peak at 1719 cm^{-1} is attributed to the carbonyl ester group (C=O). The bands at 1182cm^{-1} and 1154 $cm^{-1}$are assigned to C-O function and the peaks monitored at 1637 $cm^{-1}$and 809 cm^{-1} are relied to C=C of monomer.

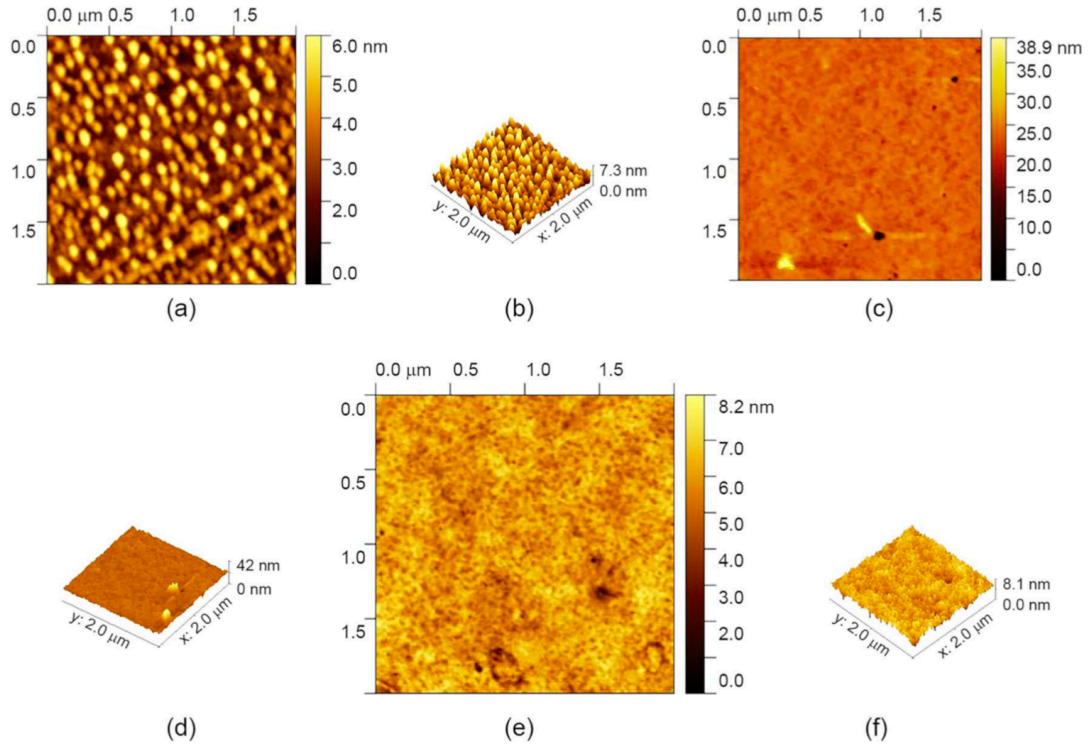

Fig. 6 AFM 2D images (first raw), 3D images (second raw), of NIP2b (**a**, **b**), NIP2a (**c**, **d**) and wMIP2a (**e**, **f**)

Fig.6 shows a clear disappearance of the C=C double bond at 1637cm^{-1} and 809cm^{-1} after 10 min of irradiation, which explains the total conversion of monomers.

ATR-FTIR spectroscopy was also used to analyze the MIP films before and after several washings to evaluate the successful insertion of PPA into the imprinted polymers and its extraction after washing. Fig.7 exhibits the

spectral differences between PPA, MIP2a, and wMIP2a. The characteristic bands of PPA at 746 cm^{-1}assigned to the aromatic C-H stretching vibrations, at 1587 cm^{-1} related to the aromatic C=C bond and at 3060 cm^{-1} characterizing the OH stretching vibrations, appear clearly in the spectra of MIP2a and disappear in that of washed MIP2a (wMIP2a). This result suggests that PPA template has been assembled and loaded during polymerization (MIP2a) and released during several washes (MIP2a).

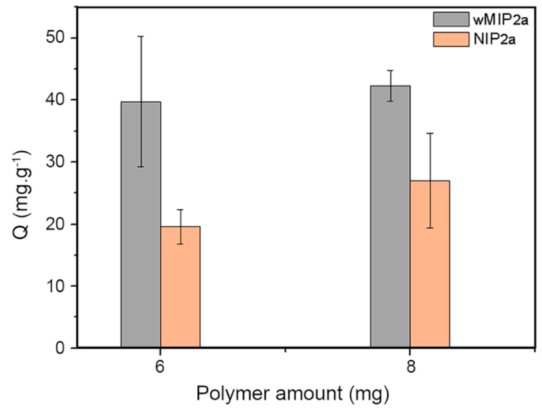

Fig. 7 Effect of film mass on adsorption capacity, [PPA] = 1.0 mg. mL^{-1}

Thermal analysis

Thermal stability and degradation stages of obtained polymers were determined using thermogravimetric analysis (TGA). The method is based on monitoring the weight of the sample during a thermal program (i.e. heating of the sample) in a controlled ambient atmosphere. Therefore, TGA was included in this study to complement and to support the interpretation of the results obtained by FTIR spectroscopy.

MIP2a, wMIP2a and NIP2a films and PPA template were heated from 25 to 700°C with a heating rate of 10°C/min and the decomposition temperature was determined from the onset of the drop in the sample weight that corresponds to the thermal decomposition. The respective thermograms are shown in Fig. 8 allowing comparison of MIP, wMIP, and NIP materials.

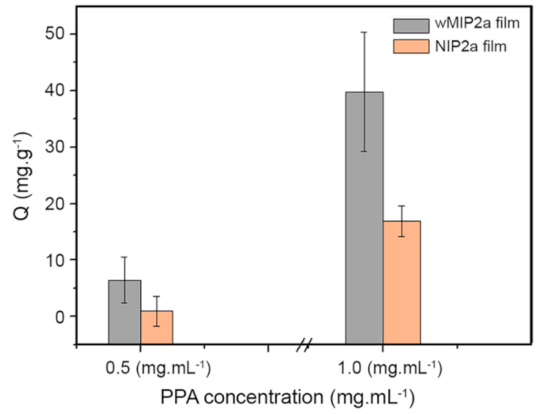

Fig. 8 Effect of PPA concentration on adsorption capacity in presence of NIP2a:wMIP2a films

As can be noticed from Fig.8, decomposition curve corresponding to MIP2a films exhibits three degradation steps. The first thermal event revealed a weight loss in the temperature range 150 - 300°C, this degradation is attributed to the PPA decomposition, which is more visible in the 156 - 304°C range in the decomposition curves of PPA when is individually analyzed.

The absence of this degradation step in the case of NIP2a, wMIP2a films confirms the absence of PAA in these films [46]. The second degradation step occurs in the temperature range of 280 - 460 °C and is shared by all systems and is attributed to the decomposition of polymers. The final degradation step, which is assigned to the degradation of organic residue at temperatures ranging from 450 to 600°C, was similar for all obtained polymers. Here it can be mentioned that the MIP2a film is the most sensitive one, due to the presence of PPA which is firstly decomposed.

AFM characterization

Scanning force microscopy (AFM) was used to investigate the surface roughness and pore creation in polymer films for NIP2a, NIP2b, and wMIP2a, in order to demonstrate the impact of the absence of porogen and template on the topographies of the films.

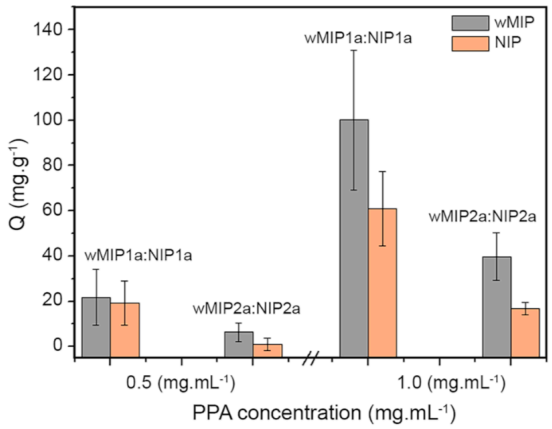

Fig. 9 Effect of cross-linking density on adsorption capacity in presence of NIP1a:wMIP1a and NIP2a:wMIP2a films

Fig. 9 depicts AFM images of NIP$_{2b}$, NIP$_{2a}$, and wMIP$_{2a}$ over a 2 x 2µm^{2}area, with the darkest regions representing the pores and the lightest regions representing the peaks [47, 48].

Fig.9 (a) and Fig. 9 (b) show 2-D and 3-D images of NIP$_{2b}$ surfaces over an area of 2 x 2µm^2. The color density depicts the vertical profile of the polymer film once more, with the peaks (highest points) appearing as light regions and the pores (valleys) appearing as small dark areas. AFM images of NIP$_{2b}$ show small grains in addition to pores, indicating that the lack of a porogenic solvent in a formulation with high crosslinker content promoted a phase separation within the network during polymerization. This phase separation was not observed in NIP$_{2a}$, which appears to be homogeneous.

The observed heterogeneity in the case of NIP$_{2b}$ suggests that the porogenic solvent is a crucial component to obtain homogeneous films. Based on these findings, we eliminated the MIP$_{2b}$ and NIP$_{2b}$ films from the recognition tests.

NIP$_{2a}$ and wMIP$_{2a}$ were characterized using AFM to demonstrate the effect of the presence of a template molecule on the topography of polymer films. From the images Fig. 9 (c) and Fig. 9 (e), it was possible to obtain the mean roughness values of the polymers using the Gwyddion AFM software. Two roughness parameters were considered in relation to the cross section profiles of the surface to quantitatively evaluate the surface properties, including the average roughness (Ra) and the root-mean-squared roughness (Rrms) which are proportional to the roughness of the surface.

Both the control and imprinted films seemed to have better surface uniformity (Figures 9(c),9(d), and 9(e), 9(f), , respectively), confirming the importance of porogenic solvent in the formation of homogeneous films.

For roughness properties, the wMIP$_{2a}$ has Ra and Rrms of about 0.511nm and 0.648nm, respectively, while the NIP$_{2a}$ has Ra and Rrms of 0.138nm and 0.181nm.

The roughness data show that the wMIP2a film is clearly rougher than the NIP2a film. This apparent roughness in the case of wMIP2a may be attributed to the cavities created by PPA molecules and thus considered as potential sites for PPA adsorption[49].

Binding properties

To show the effect of polymer amount (mg), template concentration and cross-linking density, the evaluation of wMIPs and NIPs adsorption behavior towards PPA is outlined and discussed in this study based on binding experiments [18,50,51], which is extremely useful for validating the sensing ability of MIP films. The GC technique was used for this, and all experiments were performed in triplicate and the average value was taken.

After incubation, the supernatant was collected and dried with a pump before being dissolved in 1mL of ACN containing constant concentration of heptanol for GC analysis. The equation (3) was used to calculate the concentration of PPA adsorbed in the NIP and MIP films at equilibrium.

$$Q = \frac{(C_i - C_f)\,V}{m} \qquad (3)$$

where:

- Q is the binding capacity of films, (g PPA/g film).

- C_i (g/L) and C_f (g/L) are the initial and final concentrations of PPA.

- V(L) is the initial volume of the solution.

- m (g) is the amount of the polymer film.

The imprinting effect illustrated by imprinting factor (*IF*) values was calculated as the ratio of washed imprinted polymer capacity binding Q_{wMIP} over that for non-imprinted polymer Q_{NIP}.At each rebinding test, *IF* was calculated.

$$IF = \frac{Q_{wMIP}}{Q_{NIP}} \qquad (4)$$

Because of the swelling it causes, chloroform, which is used for the formation of the complexes PPA–BuA and during the synthesis, is not used for the rebinding study. To justify the choice of this solvent, we referred to the bibliography; a review of the literature shows that acetonitrile is the most used and most appropriate solvent for rebinding tests [28,52]. This choice is based on its high polarity which allows it to interact with the target and facilitate its driving and insertion into the cavities formed during polymerization, thus increasing the specificity of the MIPs films.

Effect of polymer amount

To highlight the effect of polymer amount (mg) on the adsorption capacity of obtained polymers, a recognition study was performed for NIP2a and wMIP2a films in the presence of 1mg/mL PPA. As soon as the mass of

polymer introduced in 1 mL of the solution is less than 6 mg, it was found that the results are not reproducible and furthermore the low masses are hard to deal with; for that reason the polymer masses of 6 and 8mg were chosen to provide reproducible results and even significant adsorption capacities.

Fig.10 depicts the binding capacity of wMIP2a and NIP2a towards the PPA after six hours of incubation. It can be deduced from Fig.10 that the quantitative retention of PPA on the wMIP films is higher than that on the NIP films. This result demonstrates that the adsorption behavior of a polymer formulated with PPA differs from that of a polymer formulated identically but without it. This excess capacity demonstrated by the first polymer is widely accepted due to a population of cavities formed on the surface of this polymer that are more specific to the template. As a result, the molecular impression of MIP films is highlighted. On the other hand the NIP films allow for the quantification of non-specific interactions that occur naturally on its surface. Theoretical investigations conducted by et al confirms that MIP polymers have more uniform binding site energies, and these sites have higher affinities and stronger binding energies to analytes.Hijazi, H. Y., & Bottaro, C. S. (2020). Molecularly imprinted polymer thin-film as a micro-extraction adsorbent for selective determination of trace concentrations of polycyclic aromatic sulfur heterocycles in seawater. *Journal of Chromatography A*, *1617*, 460824. Recently Neusser et al. have reported differences in the interconnection of pores between MIPs and NIPs. The team used 3D FIB/SEM tomography to examine the porosity of MIPs, and they discovered that MIPs had more interconnected pores than NIPs, which had smaller interconnection areas. It was observed that the pore volume of MIPs was respectively 34% and 35% higher than those of the NIPs. The high pore size for MIPs supports the formation of specific cavities inside the polymer matrix due to the use of a template during polymerization.

Fig.10 also shows that the amount of polymer has a significant effect on the adsorption capacity of the wMIP films. The adsorption capacity of the wMIP films for PPA increased sharply when the polymer amount was increased from 6 to 8 mg at the studied template concentration.

The increase in adsorption capacity with increasing polymer concentration is expected due to an increase in the number of effective binding sites.

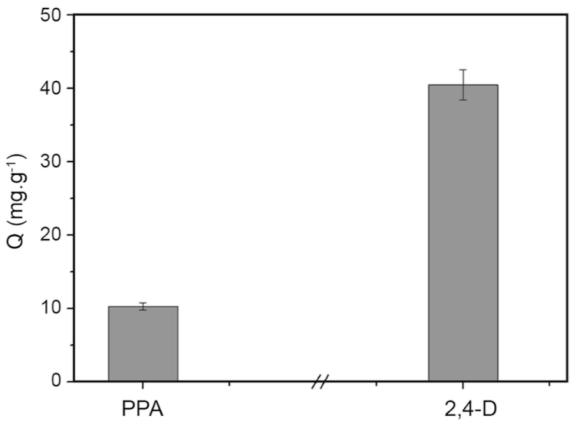

Fig. 10 Selectivity of wMIP2a towards PPA and 2,4-D

Table 4 Binding capacities and imprinting factors for wMIP2a:NIP2a polymer films

Polymer amount (mg)	Q (mg.g^{-1})		
	wMIP2a	NIP2a	IF
6	39.75	16.87	2.35
8	42.31	26.45	1.59

According to the *IF* value given on Table 4, the wMIP2a with a polymer mass of 6mg has the highest imprinting factor. This result can be explained by an increase in the number and distribution of binding sites as the amount of polymer increases, which subsequently promotes the adsorption of PPA molecules on both specific and non-specific binding sites.

Obviously, 6mg is the appropriate amount of polymer for this; it was chosen as the optimal adsorbent amount for the recognition test, which is presented in the following section.

Effect of PPA concentration

In order to show the effect of PPA concentration on the absorption capacity of NIP2a and wMIP2a films, a mass of 6mg of NIP2a :wMIP2a was put in acetonitrile solutions of PPA 0.5mg mL^{-1} and 1 mg mL^{-1}, respectively.

Fig.11 illustrates the amount of PPA bound to wMIP2a and NIP2a films in presence of two PPA concentrations 0.5 and 1mg mL^{-1}.

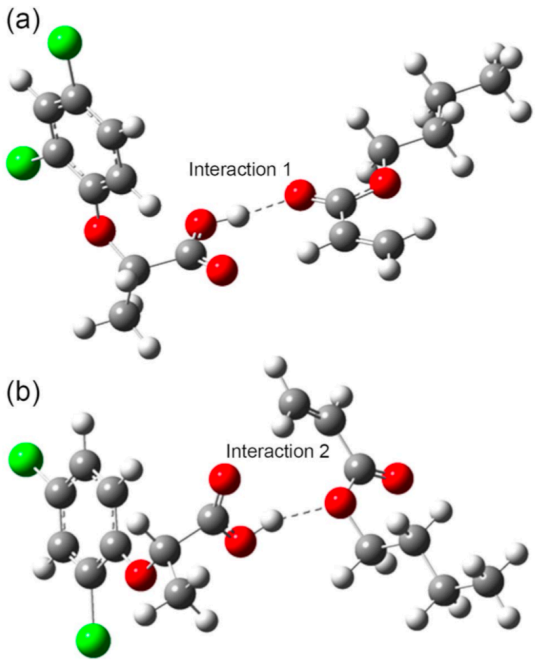

Fig. 11 DFT-B3LYP/6-31G (d, p) optimized geometries of complexes 1b (**a**) and 2b (**b**)

The imprinted films fixed or adsorbed more PPA than the non-imprinted films for the both concentrations, confirming the successful imprinting process. The amount of PPA in NIP and wMIP increases with PPA concentration.

The presence of specific and non-specific binding sites is one of the most significant drawbacks of the non-covalent approach; this heterogeneity has an important impact on the impression properties of MIPs. As a result, the increase of adsorption capacities with increasing the PPA concentration is due to the adsorption of PPA on both high and low affinity binding sites [52]. To better show the efficiency of the MIP over the NIP; Table5 summarizes the imprinting factors of each experiment.

Table 5 Binding capacities and imprinting factors for wMIP1a:NIP1a and wMIP2a:NIP2a polymer films

Adsorbent	Q (mg.g^{-1})	IF
[PPA] = 0.5 (mg.mL^{-1})		
wMIP1a	21.86	1.14
NIP1a	19.17	
wMIP2a	6.43	6.77
NIP2a	0.95	
[PPA] = 1.0 (mg.mL^{-1})		
wMIP1a	100.49	1.64
NIP1a	60.96	
wMIP2a	39.74	2.35
NIP2a	16.87	

Typically, a high *IF* value indicates the efficiency of the imprinting method and demonstrates that the selective interactions exceed the capacities of non-selective adsorption within the polymer films.

As a result, the decrease of *IF* values with increasing PPA concentration (Table 5) is due to heterogeneous binding on the available sites (printed and non-printed), resulting in non-specific adsorption. These findings also confirm that at low PPA concentrations, PPA's affinity to bind on specific sites exceeds non specific binding[21, 53].

Effect of the crosslinking density

To underline the effect of the crosslinking density in binding tests, recognition studies have been carried out in presence of NIP1a:wMIP1a and NIP2a:wMIP2a for PPA concentration of 0.5mg mL^{-1} and 1 mg mL^{-1}, respectively. The binding capacities of NIP1a:wMIP1a and NIP2a:wMIP2a films are presented in Fig.12 which shows a significant difference in the retention capacity between MIPs and NIPs for both studied crosslinking densities and concentrations. It suggests the high efficiency of the imprinting process since the amount of PPA adsorbed in the presence of wMIP1a/NIP1a films was approximately two times higher than that adsorbed by MIP2a:NIP2a films.

This could be attributed to the stiffness of the polymers formed in the presence of high crosslinking density in the case of wMIP2a:NIP2a, which may limit the diffusion of PPA molecules to the polymers. This result is consistent with other findings showing that the adsorption capacity of polymers increases as cross-linking density decreases [34]. One the other hand, the *IF* for NIP2a:MIP2a is much higher than the *IF* for NIP1a:MIP1a.All values are gathered in Table 6.

Because of the stabilization of imprinted polymer recognition sites, polymers with a high crosslinking density are expected to have the highest *IF*. Selectivity is also generally favored in the presence of high crosslinker content due to the preservation of cavity shape after the template is removed.

It's worth noting that this study showed that using a low amount of crosslinker can have an imprinting effect even though the high ratio template/monomer/crosslinker (1:4:20) is widely employed, in the creation of MIPs. In addition, the template/monomer/cross-linker (1:4:8) gives films displaying good binding behavior for 2,4 D analogue. Thus the preparation of thin films based on acrylate could be promising potentials for the development and the fabrication of sensors or other applications.

Table 6 Computational modeling data for complexes template-monomer 1b and 2b: binding energy, ΔE (kcal./mol), and bond length, r(Å)

	r_{O-H} (Å)	$r_{O...H}$ (Å)	Binding energy ΔE (kcal./mol)	Stabilization energy $\Delta E^{(2)}$ (kcal/mol)
(RCO_2H)	0.976	–	–	
Complex 1b	0.997	1.738	−15.28	LP(2 s) $O_{(C=O)} \rightarrow \sigma^*$ O–H: 10.17 LP(2p) $O_{(C=O)} \rightarrow \sigma^*$ O–H: 17.44
Complex 2b	0.988	1.849	−09.92	LP(2 s) $O_{(C-O)} \rightarrow \sigma^*$ O–H: 11.17 LP(2p) $O_{(C-O)} \rightarrow \sigma^*$ O–H: 04.02

Conclusions

The current study optimized the conditions for herbicide analogue imprinting. Computer modeling, and ^{1}H-NMRanalysis have all been used to demonstrate the existence of a hydrogen binding interaction between PPA as a 2,4-D analogue and BuA as a functional monomer.

The development of porous imprinted films and their non-imprinted polymers was carried out by the sandwich method in the presence of a porogen solvent which is chloroform, in order to develop selective cavities towards the PPA.

Interestingly, the obtained thin films were characterized by ATR-FTIR, TGA and AFM. Two main conclusions could be drawn from IR spectra: first, total polymerization of pre-polymerization mixture was obtained; second, the template molecule was successfully removed from MIP polymers. The AFM images provided useful information about the effect of the porogenic solvent on the final topography of the resulting materials. TGA analysis revealed that all polymers degrade in the same way and that the presence of PPA in imprinted polymers affects their thermal stability. Overall, adsorption experiment results show that the retention capacity of wMIPs was higher than that of the NIPs. Additionally, a decrease of imprinting factors (*IF*) was noticed as the PPA concentration increases. In addition, polymer films obtained with high crosslinking density exhibit a good imprinting effect.

Declaration of competing interest

The authors declare that they have no known competing financial interests or personal relationships that could have appeared to influence the work reported in this paper.

Acknowledgements

The authors gratefully acknowledge the support of the Algerian Ministry of Higher Education and Scientific Research (MESRS), the General Directorate of Scientific Research and Technological Development (DGRSDT) of Algeria, and the University of Tlemcen in Algeria,

References.

1. De Amarante Jr OP, Brito NM, dos Santos TCR, Nunes GS and Ribeiro ML (2003) Determination of 2, 4-dichlorophenoxyacetic acid and its major transformation product in soil samples by liquid chromatographic analysis. Talanta 60:115-121

2. Jiang X, Li D, Xu X, Ying Y, Li Y, Ye Z and Wang J (2008) Immunosensors for detection of pesticide residues. Biosensors and Bioelectronics 23:1577-1587
3. Dehnert GK, Freitas MB, DeQuattro ZA, Barry T and Karasov WH (2018) Effects of low, subchronic exposure of 2, 4-Dichlorophenoxyacetic acid (2, 4-D) and commercial 2, 4-D formulations on early life stages of fathead minnows (Pimephales promelas). Environmental toxicology and chemistry 37:2550-2559
4. Islam F, Farooq MA, Gill RA, Wang J, Yang C, Ali B and Zhou W (2017) 2,4-D attenuates salinity-induced toxicity by mediating anatomical changes, antioxidant capacity and cation transporters in the roots of rice cultivars. Scientific reports 7:10443
5. Lajmanovich RC, Attademo AM, Simoniello MF, Poletta GL, Junges CM, Peltzer PM and Cabagna-Zenklusen MC (2015) Harmful effects of the dermal intake of commercial formulations containing chlorpyrifos, 2, 4-D, and glyphosate on the common toad Rhinella arenarum (Anura: Bufonidae).Water, Air and Soil Pollution 226: 1-12
6. Abigail M, Samuel SM, Needhidasan S, Ramalingam C (2017) Stratagems employed for 2,4-dichlorophenoxyacetic acid removal from polluted water sources. Clean Technol Environ Policy 19:1607-1620
7. De Castro Marcato AC, De Souza CP and Fontanetti CS (2017) Herbicide 2, 4-D: a review of toxicity on non-target organisms. Water Air Soil Pollut 228:1-12
8. Sheng L, Jin Y, He Y, Huang Y, Yan L, and Zhao R (2017) Well-defined magnetic surface imprinted nanoparticles for selective enrichment of 2, 4-dichlorophenoxyacetic acid in real samples. Talanta 174 :725-732
9. Song Y, Ma R, Hao L, Yang X, Wang C, Wu Q and Wang Z (2018) Application of covalent organic framework as the adsorbent for solid-phase extraction of trace levels of pesticide residues prior to high-performance liquid chromatography-ultraviolet detection. Journal Chromatography A 1572:20-26
10. Bogialli S, Curini R, Di Corcia A, Laganà A, Stabile A and Sturchio E (2006) Development of a multiresidue method for analyzing herbicide and fungicide residues in bovine milk based on solid-phase extraction and liquid chromatography–tandem mass spectrometry. Journal Chromatography A 1102:1-10
11. Figueiredo L, Erny GL, Santos L and Alves A (2016) Applications of molecularly imprinted polymers to the analysis and removal of personal care products: A review. Talanta 146:754-765
12. Wang X, Qiu G, Ge Y, Zheng W, Peng Y and Fei D (2020) In situ preparation of magnetic molecularly imprinted polymer particles utilizing moulding particles. Bulletin of Materials Science 43:1-8

13. Wang Y, Wang E, Wu Z, Li H, Zhu Z, Zhu X and Dong Y (2014) Synthesis of chitosan molecularly imprinted polymers for solid-phase extraction of methandrostenolone. Carbohydrate polymers 101:517-523
14. Soleimani M, and Faghihi K (2020) Selective adsorption of ketoconazole from aqueous solutions using a new molecularly imprinted polyurethane coated magnetic multiwall carbon nanotubes. Iranian Polymer Journal 29:785-798
15. Lenain P, Diana D, Mavungu J, Dubruel P, Robbens J and De Saeger S (2012) Development of suspension polymerized molecularly imprinted beads with metergoline as template and application in a solid phase extraction procedure towards ergot alkaloids. Analytical chemistry 84:10411-10418
16. Liu X, Wang Y, Wang J, Li L and Li R (2019) Hydrophilic molecularly imprinted dispersive solid-phase extraction coupled with liquid chromatography for determination of azoxystrobin residues in cucumber. Iranian Polymer Journal 28:725-734
17. Pluhar B, Ziener U and Mizaikoff B (2013) Surface imprinting of pepsin via emulsion polymerization. Journal of Materials Chemistry B 1:5489-5495
18. Hijazi HY and Bottaro CS (2020) Molecularly imprinted polymer thin-film as a micro-extraction adsorbent for selective determination of trace concentrations of polycyclic aromatic sulfur heterocycles in seawater. Journal of Chromatography A 1617: 460824
19. Mohseni E, Yaftian M R, Shayani-jam H, Zamani A and Piri F (2020) Molecularly imprinted poly (4, 4′-methylenedianiline) for selective electrochemical detection of dibenzothiophene. Iranian Polymer Journal 29:403-409
20. Rico-Yuste A and Carrasco S (2019) Molecularly imprinted polymer-based hybrid materials for the development of optical sensors. Polymers 11: 1173
21. Schmidt RH, Belmont AS and Haupt K (2005) Porogen formulations for obtaining molecularly imprinted polymers with optimized binding properties. Analytica chimica acta 542:118-124
22. Gryshchenko AO and Bottaro CS (2014) Development of molecularly imprinted polymer in porous film format for binding of phenol and alkylphenols from water. International Journal of Molecular Sciences 15:1338-1357
23. Zhang H, Song T, Zhang W, Hua W and Pan C (2007) Retention behavior of phenoxyacetic herbicides on a molecularly imprinted polymer with phenoxyacetic acid as a dummy template molecule. Bioorganic and medicinal chemistry 15:6089-6095

24. Bagheri AR, Arabi M, Ghaedi M, Ostovan A, Wang X, Li J and Chen L (2019) Dummy molecularly imprinted polymers based on a green synthesis strategy for magnetic solid-phase extraction of acrylamide in food samples. Talanta 195:390-400
25. Zhang Z, Cao X, Zhang Z, Yin J, Wang D, Xu Y, Zheng W, Li X, Zhang Q and Liu L (2020) Synthesis of dummy-template molecularly imprinted polymer adsorbents for solid phase extraction of aminoglycosides antibiotics from environmental water samples. Talanta 208 :120385
26. Utami AR, Zulfikar MA and Wahyuningrum D (2021) The synthesis of magnetic molecularly imprinted polymer against di-(2-ethylhexyl) phthalate. IOP Conference Series Materials Science and Engineering 1143: 012003
27. Laskar N, Ghoshal D and Gupta S (2021) Chitosan-based magnetic molecularly imprinted polymer: synthesis and application in selective recognition of tricyclazole from rice and water samples. Iranian Polymer Journal 30: 121-134
28. Simões M, Martins N, Cabrita MJ, Burke AJ and Garcia R (2014) Tailor-made molecularly imprinted polymers for dimethoate and deltamethrin recognition: synthesis, characterization and chromatographic evaluation. Journal of Polymer Research 21:1-13
29. Mirzajani R, Ramezani Z and Kardani F (2017) Selective determination of thidiazuron herbicide in fruit and vegetable samples using molecularly imprinted polymer fiber solid phase microextraction with ion mobility spectrometry detection (MIPF-SPME-IMS). Microchemical Journal 130:93-101
30. Hasanah AN, Fauzi D, Witka BZ, Rahayu D and Pratiwi R (2020) Molecular Imprinted Polymer for Ethylmorphine with Methacrylic Acid and Acrylamide as Functional Monomer in Butanol Using Two Polymerization Method. Mediterranean Journal of Chemistry 10:277-288
31. Aguilar J F, Miranda J M, Rodriguez J A, Paez-Hernandez M E and Ibarra I S (2020) Selective removal of tetracycline residue in milk samples using a molecularly imprinted polymer. Journal of Polymer Research 27:1-12
32. Lin Y, Liu Y, Li S, Rui L, Ou J, Wu Q and He J (2021) Template-directed preparation of three-dimensionally ordered macroporous molecularly imprinted microspheres for selective recognition and separation of quinine from cinchona extract. Journal of Polymer Research 28:1-10
33. Mbhele ZE, Ncube S and Madikizela LM (2018) Synthesis of a molecularly imprinted polymer and its application in selective extraction of fenoprofen from wastewater .Environmental Science and Pollution Research 25:36724-36735

34. Hung CY, Huang YT, Huang HH and Hwang CC (2006) Preparation of (S)-ibuprofen-imprinted polymer and its molecular recognition study. Journal of Applied Polymer Science 102:2972-2979

35. Frisch MJ, Trucks GW, Schlegel HB, Scuseria GE, Robb MA, Cheeseman JR and Fox DJ (2009) Gaussian 09 Revision D. 01 Gaussian Inc, Wallingford CT

36. Becke ADJ (1993) Density-functional thermochemistry. III. The role of exact exchange. Journal of Chemical Physics 98: 5648-5652

37. Lee C, Yang W, Parr R G (1988) Development of the Colic-Salvetti correlation-energy formulation a functional of the electron density. Physical Review B 37: 785-789

38. Tang K, Gu X, Luo Q, Chen S, Wu L and Xiong J (2014) Preparation of molecularly imprinted polymer for use as SPE adsorbent for the simultaneous determination of five sulphonylurea herbicides by HPLC. Food chemistry 150:106-112

39. Andersson HS, Karlsson JG, Piletsky SA, Koch-Schmidt AC, Mosbach K and Nicholls IA (1999)Study of the nature of recognition in molecularly imprinted polymers, II: influence of monomer–template ratio and sample load on retention and selectivity. Journal of Chromatography A 848:39-49

40. Annamma KM and Beena M (2011) Design of 2, 4-dichlorophenoxyacetic acid imprinted polymer with high specificity and selectivity. Materials Sciences and Applications 2:131-140

41. Sajini T, Thomas R and Mathew B (2019) Rational design and synthesis of photo-responsive molecularly imprinted polymers for the enantioselective intake and release of L-phenylalanine benzyl ester on multiwalled carbon nanotubes. Polymer 173:127-140

42. Wu L, Zhu K, Zhao M and Li Y (2005) Theoretical and experimental study of nicotinamide molecularly imprinted polymers with different porogens. Analytica chimica acta 549:39-44

43. Hawari HF, Samsudin NM, Shakaff AM, Wahab Y, Hashim U, Zakaria, A and Ahmad, MN (2013) Highly selective molecular imprinted polymer (MIP) based sensor array using interdigitated electrode (IDE) platform for detection of mango ripeness. Sensors and Actuators B: Chemical 187:434-444

44. Tarannum N and Singh M (2011)Selective recognition and detection of l-aspartic acid by molecularly imprinted polymer in aqueous solution. American Journal of Analytical Chemistry 2:909-918

45. Vendamme R, Eevers W, Kaneto M and Minamizaki Y (2009) Influence of polymer morphology on the capacity of molecularly imprinted resins to release or to retain their template. Polymer journal 41:1055-1066

46. Dima ŞO, Nicolae CA, Lordache TV, Chetraru O, Meouche W, Faraon VA and Donescu D (2015) Thermal analyses as tools for proving the molecular imprinting with diosgenin and sclareol in acrylic copolymer matrices. Journal of Thermal Analysis and Calorimetry 120:1107-1118
47. Hilal N, Kochkodan V, Al-KhatibL and Busca G (2002) Characterization of molecularly imprinted composite membranes using an atomic force microscope. Surface and interface analysis 33:72-675
48. Campbell SE, Collins M, Xie L and BelBruno JJ (2009) Surface morphology of spin-coated molecularly imprinted polymer films. Surf. Interface Anal 41:347-356
49. El Kirat K, Bartkowski M and Haupt K (2009) Probing the recognition specificity of a protein molecularly imprinted polymer using force spectroscopy. Biosensors and Bioelectronics 24:2618-2624
50. Song D, Zhang Y, Geer MF and Shimizu KD (2014) Characterization of molecularly imprinted polymers using a new polar solvent titration method. Journal of Molecular Recognition 27:448-457
51. Spivak DA (2005) Optimization, evaluation, and characterization of molecularly imprinted polymers. Advanced drug delivery reviews 57:1779-1794
52. Hillberg AL, Brain KR and Allender CJ (2009) Design and evaluation of thin and flexible theophylline imprinted polymer membrane materials. Journal of Molecular Recognition 22:223-231
53. Dima SO, Meouche W, Dobre T, Nicolescu TV and Sarbu A (2013) Diosgenin-selective molecularly imprinted pearls prepared by wet phase inversion. Reactive and Functional Polymers 73:1188-1197